Naval Research Laboratory

Washington, DC 20375-5320

NRL/MR/7220--14-9558

Analysis of the WindSat Receiver Frequency Passbands

Michael H. Bettenhausen
Peter W. Gaiser

Remote Sensing Physics Branch
Remote Sensing Division

September 12, 2014

REPORT DOCUMENTATION PAGE

Form Approved
OMB No. 0704-0188

1. REPORT DATE *(DD-MM-YYYY)*
12-09-2014

2. REPORT TYPE
Memorandum Report

3. DATES COVERED *(From - To)*
October 2013 – July 2014

4. TITLE AND SUBTITLE
Analysis of the WindSat Receiver Frequency Passbands

5a. CONTRACT NUMBER

5b. GRANT NUMBER

5c. PROGRAM ELEMENT NUMBER

6. AUTHOR(S)
Michael H. Bettenhausen and Peter W. Gaiser

5d. PROJECT NUMBER

5e. TASK NUMBER

5f. WORK UNIT NUMBER

7. PERFORMING ORGANIZATION NAME(S) AND ADDRESS(ES)
Naval Research Laboratory
4555 Overlook Avenue, SW
Washington, DC 20375-5350

8. PERFORMING ORGANIZATION REPORT NUMBER
NRL/MR/7220--14-9558

9. SPONSORING / MONITORING AGENCY NAME(S) AND ADDRESS(ES)
Naval Research Laboratory
4555 Overlook Avenue, SW
Washington, DC 20375-5350

10. SPONSOR / MONITOR'S ACRONYM(S)

11. SPONSOR / MONITOR'S REPORT NUMBER(S)

12. DISTRIBUTION / AVAILABILITY STATEMENT
Approved for public release; distribution is unlimited.

13. SUPPLEMENTARY NOTES

14. ABSTRACT
The WindSat instrument is the primary payload for the Coriolis mission which was launched on 6 January 2003. WindSat is a 22-channel conical-scanning radiometer which measures the vertical and horizontal polarizations at nominal center frequencies of 6.8 and 23.8 GHz and six polarizations at nominal center frequencies of 10.7, 18.7, and 37 GHz. The prelaunch WindSat receiver frequency passband measurements are presented and modeled with a functional fit. Radiative transfer simulations are presented which model the differences between the measured brightness temperatures for ocean scenes and the simulated brightness temperatures for the nominal design receiver frequency passbands. Significant differences are shown for the channels with 18.7 and 23.8 GHz nominal center frequencies. These differences are shown to be a function of the precipitable water vapor in the measured scene.

15. SUBJECT TERMS
WindSat, Receiver, Radiative transfer, Microwave, Passband

16. SECURITY CLASSIFICATION OF: a. REPORT	b. ABSTRACT	c. THIS PAGE	17. LIMITATION OF ABSTRACT	18. NUMBER OF PAGES	19a. NAME OF RESPONSIBLE PERSON
Unclassified Unlimited	Unclassified Unlimited	Unclassified Unlimited	Unclassified Unlimited	17	Michael H. Bettenhausen
					19b. TELEPHONE NUMBER *(include area code)* (202) 767-8278

Standard Form 298 (Rev. 8-98)
Prescribed by ANSI Std. Z39.18

CONTENTS

FIGURES

TABLES

ANALYSIS OF THE WINDSAT RECEIVER FREQUENCY PASSBANDS

1. INTRODUCTION

The WindSat instrument is the primary payload for the Coriolis mission which was launched on 6 January 2003. WindSat is a 22-channel conical-scanning radiometer which measures the vertical and horizontal polarizations at nominal center frequencies of 6.8 and 23.8 GHz and six polarizations (vertical (V), horizontal (H), $+45^\circ$ linear (P), -45° linear (M), left circular (L) and right circular (R)) at nominal center frequencies of 10.7, 18.7 and 37 GHz.

The WindSat receiver subsystem is divided into three units: the front-end receiver (FER), the receiver electronics unit (REU) and the detector electronics unit (DEU). A more detailed description of the WindSat instrument and the receiver subsystem can be found in Gaiser, et al. [1]. The receiver frequency passband response is primarily determined by the band pass filter in the REU. The characteristics of the frequency passband responses can have a significant effect on the measured brightness temperatures (T_b's) [2].

2. MEASURED RECEIVER PASSBANDS

The WindSat receiver frequency passband responses were measured pre-launch at three different temperatures: 0, 25 and 40°C. The only passband measurements currently available for channels with a nominal center frequency of 10.7 GHz are those taken at 25°C. Passband measurements are available at all three temperatures for all other channels.

The passband measurements provide receiver frequency passband responses for each WindSat receiver at 401 evenly-spaced frequencies over the passband. The measurement frequencies were consistent for all channels with the same nominal center frequency. Figure 1 shows the receiver passband responses for all five WindSat vertically polarized channels. The range of frequencies over which the receiver passband responses were measured correspond to the minumum and maximum values shown on the frequency axes of the plots. Figure 1 also shows fits to the measured passband response of the form [2]

$$H_{\text{fit}} = \frac{A(B/2)^\alpha}{|\nu-\nu_0|^\alpha + (B/2)^\alpha \left[1 + a\frac{(\nu-\nu_0)}{(10^9\text{Hz})}\right]} \tag{1}$$

where the fit parameters are center frequency, ν_0, the bandwidth, B, α, and a. The sharpness of the edges of the passband fit is determined by α. The factor a models asymmetry of the passband response about ν_0. The passband responses were scaled so that $A = 1$. The fits were derived by using a Nelder-Mead algorithm [3, 4] to solve for the Equation (1) parameters which minimize

$$\sum_i (H_{\nu,i} - H_{\text{fit},i})^2 . \tag{2}$$

Manuscript approved August 11, 2014.

where $H_{\nu,i}$ is the measured passband response at frequency i and $H_{\mathrm{fit},i}$ is the value of the fit at that frequency. Table 1 gives the fit parameters for all 22 WindSat receiver passbands. Section 3 describes a method for modeling the T_b's integrated over the receiver frequency passband for a set of atmospheric profiles. The ν_0 column in Table 1 gives the values which result from minimization of Equation (2) with small adjustments to remove (<0.35 K) biases in the modeled T_b's when using the fits for the passbands. These adjustments to ν_0 were calculated using a one-dimensional bracketing optimization to reduce the biases to less than 0.01 K. The receiver passband response fits produced using the parameters given in Table 1 are shown in Figure 2 for each WindSat frequency band.

Table 1: Optimized fit parameters for the WindSat receiver passbands using the functional form given in Equation (1).

Channel	T_{REU} (°C)	ν_0(GHz)	B (MHz)	α	a
6.8 V	0	6.804	125.7	14.359	0.3801
	25	6.800	126.4	15.241	0.4492
	40	6.798	126.5	15.406	0.4972
6.8 H	0	6.803	122.7	12.156	0.0920
	25	6.801	122.4	11.666	0.0090
	40	6.799	122.3	11.565	-0.0207
10.7 V	25	10.700	308.4	11.104	-0.7149
10.7 H	25	10.704	305.5	12.130	-0.6207
10.7 P	25	10.703	305.1	12.304	-0.4119
10.7 M	25	10.693	308.4	11.965	-0.6213
10.7 L	25	10.700	320.3	14.542	-0.4070
10.7 R	25	10.710	305.7	9.813	-0.4244
18.7 V	0	18.732	705.4	7.555	0.2030
	25	18.687	695.6	7.311	0.2614
	40	18.691	729.0	9.243	0.1767
18.7 H	0	18.759	775.3	10.492	-0.0998
	25	18.742	766.3	9.706	0.0454
	40	18.734	760.9	9.269	0.1184
18.7 P	0	18.728	758.3	12.664	-0.2920
	25	18.716	758.1	12.688	-0.2857
	40	18.712	755.7	12.597	-0.3059
18.7 M	0	18.720	775.7	13.178	0.0020
	25	18.707	777.7	13.344	-0.0052
	40	18.704	778.6	13.412	0.0100
18.7 L	0	18.725	738.8	9.870	0.3491
	25	18.712	731.4	9.809	0.3930
	40	18.708	729.8	9.745	0.4035
18.7 R	0	18.721	774.1	10.634	0.1048
	25	18.703	757.4	9.507	0.0409
	40	18.695	747.9	8.968	0.0443

Table 1: (continued)

Channel	T_{REU} (°C)	ν_0(GHz)	B (MHz)	α	a
23.8 V	0	23.802	499.0	7.646	-0.3708
	25	23.787	493.9	7.943	-0.1666
	40	23.777	490.2	8.249	-0.0772
23.8 H	0	23.807	510.5	5.828	-0.7423
	25	23.793	503.8	5.731	-0.6026
	40	23.781	503.5	5.725	-0.5079
37 V	0	37.025	1991.7	12.431	0.0585
	25	37.006	1955.2	10.984	-0.0810
	40	36.999	1946.9	10.372	-0.0688
37 H	0	36.968	1996.6	11.248	-0.2271
	25	36.951	1944.8	7.561	-0.3128
	40	36.942	1970.4	8.306	-0.2279
37 P	0	37.023	1801.3	7.213	0.0207
	25	36.999	1734.1	6.268	-0.0564
	40	36.989	1752.3	6.337	-0.0812
37 M	0	37.028	2008.9	18.472	-0.1300
	25	37.007	2006.6	17.059	-0.1352
	40	37.007	1997.9	15.277	-0.0888
37 L	0	37.006	1842.9	8.819	-0.2001
	25	36.982	1797.0	7.304	-0.2805
	40	36.973	1751.9	6.097	-0.3281
37 R	0	36.980	1956.2	10.761	-0.0537
	25	36.961	1910.2	8.300	-0.1213
	40	36.945	1854.9	6.361	-0.2148

3. MODELING RESULTS

The results presented here were obtained using the analysis method described in [2]. The T_b is calculated by integrating the product of the measured receiver response H_ν, or an idealized receiver response, and the modeled monochromatic brightness temperature ($T_{b,\nu}$) over the receiver passband.

$$T_b = \frac{\int_0^\infty d\nu T_{b,\nu} H_\nu}{\int_0^\infty d\nu H_\nu} \tag{3}$$

The radiative transfer model used to calculate $T_{b,\nu}$ combines the monochromatic radiative transfer model MonoRTM [5] with the Fresnel reflectivities for a specular sea surface obtained using the permittivity model for sea water developed by Stogryn [6]. The T_b are modeled for the WindSat channels using a selected subset of atmospheric profiles assembled by the Satellite Application Facility for Numerical Weather Prediction (NWP SAF) [7]. The subset was chosen to provide a diverse set of temperature, water vapor and cloud liquid water profiles while excluding most precipitation. The atmospheric profile set and the radiative transfer model are described in more detail in [2].

Radiative transfer modeling of WindSat T_b's previously assumed idealized receiver frequency passband responses. For example, the forward model used for the ocean surface vector wind retrievals described in [8] assumed monochromatic passbands at the nominal center frequencies. Figure 3 shows differences between T_b's calculated using the measured passbands for 25 °C receiver temperature and T_b's calculated assuming monochromatic receiver responses at the nominal center frequencies. Significant differences are shown for the 18.7, 23.8 and 37 GHz bands. Differences for the 6.8 GHz band (not shown) are negligible (< 0.005 K). The differences in Figure 3 are plotted versus the precipitable water vapor (PWV) calculated for each atmospheric profile. The differences for the 18.7 and 23.8 GHz bands vary with PWV.

Modeled T_b's for receiver passbands using the functional fits per Equation (1) and Table 1 agree with modeled T_b's using the measured receiver passbands to better than 0.01 K for all profiles and all channels. However, the functional fits for the receiver responses are difficult to apply for fast radiative transfer calculations. It can also be difficult to understand the importance of the differences between the receiver responses for different channels and temperatures from the functional fits. An alternative is to use a monochromatic model with the frequency shifted to best match the T_b's obtained using the measured passbands. The T_b's obtained using optimized monochromatic models are accurate to within 0.1 K for the 23.8 GHz horizontal polarization and to within 0.04 K for all other channels. The optimized frequency for the monochromatic model for each channel is given in Table 2 corresponding to the receiver passband measurements at 0, 25 and 40 °C.

The measured receiver passband responses clearly change with temperature as shown by the results Table 1 and 2. Table 3 provides one measure of the importance of these differences. The results show that the differences due to changes in the receiver temperature can be significant, although small, for the 18.7 GHz, 23.8 GHz and, to a lesser extent, the 37 GHz channels. The differences due to temperature are insignificant for the 6.8 GHz channels. It is also likely that receiver temperature effects are not significant for the 10.7 GHz channels based on the results for the other frequency bands.

The WindSat REU on-orbit temperatures have stayed in the range of about 24–39 °C throughout the mission as shown in Figure 4. This justifies only considering the 25 and 40 °C receiver temperatures for Table 3. The lowest REU temperatures are for the 10.7 GHz V/H REU and the highest are for the 37 GHz P/M REU. The REU temperatures for the other channels are displayed in light gray to show that the shape of the temperature distribution is similar for all channels. REU temperature varies primarily with solar illumination of the instrument. The temperature variations exhibit both annual and orbital cycles as shown in Figures 5 – 6, respectively. The 6.8 GHz receivers were turned off over the range of days 1956 to 1977 shown in Figure 5 which reduced the heat generated by WindSat and lowered the REU temperatures during that time period. Orbital variation is smallest in late February and largest in late May. The variations for separate orbits on the same day show only small differences under normal WindSat operating conditions.

4. CONCLUSIONS

The WindSat receiver frequency passbands differ significantly from the nominal design for the instrument. Most importantly there are differences in the passbands within the same frequency band that can impact the measured T_b's particularly for the 18.7 GHz frequency band. These differences will impact measurement of the third and fourth Stokes parameters which rely on matching between the P/M and L/R polarization pairs. As shown in Figure 3 the impact on the T_b's varies primarily with the water vapor in the measurement scene. Additionally, receiver temperature changes can also modify the measured T_b's particularly for the H-polarization channels at 18.7 and 23.8 GHz.

Table 2 — Frequencies in GHz for monochromatic modeling of the WindSat channel set based on radiative transfer calculations using receiver frequency passband measurements at 0, 25 and 40 °C.

Channel	0 °C	25 °C	40 °C
6.8 V	6.804	6.801	6.799
6.8 H	6.804	6.801	6.799
10.7 V	-	10.705	-
10.7 H	-	10.708	-
10.7 P	-	10.706	-
10.7 M	-	10.699	-
10.7 L	-	10.704	-
10.7 R	-	10.713	-
18.7 V	18.734	18.688	18.694
18.7 H	18.774	18.751	18.740
18.7 P	18.749	18.737	18.734
18.7 M	18.730	18.717	18.714
18.7 L	18.722	18.707	18.703
18.7 R	18.727	18.712	18.704
23.8 V	23.809	23.790	23.779
23.8 H	23.820	23.803	23.790
37 V	37.018	37.037	37.027
37 H	37.054	37.056	37.028
37 P	37.031	37.024	37.020
37 M	37.082	37.062	37.048
37 L	37.065	37.057	37.055
37 R	37.011	37.010	37.017

The analysis and effects discussed in this report apply only to non-precipitation ocean scenes. The effects are less significant for other surface types (land, sea ice, snow) because atmospheric effects are less important for those scenes. Additionally, for sea ice and snow the water vapor is in the lower part of the global water vapor range which further limits the effect on the T_b's.

Caution must be used when applying the modeling results presented here to analysis of on-orbit WindSat data. The results here are solely based on radiative transfer modeling using pre-launch receiver characteristics. It is not known how accurately the pre-launch characteristics match with the on-orbit receiver characteristics throughout the mission.

Table 3 — The maximum difference between the calculated T_b's using the measured receiver passbands for receiver temperatures of 25 °C ($T_{b,25}$) and 40 °C ($T_{b,40}$).

Channel	$\max(\lvert T_{b,40} - T_{b,25}\rvert)$ (K)
18.7 V	0.08
18.7 H	0.27
18.7 P	0.07
18.7 M	0.06
18.7 L	0.08
18.7 R	0.15
23.8 V	0.13
23.8 H	0.29
37 V	0.02
37 H	0.10
37 P	0.01
37 M	0.04
37 L	0.01
37 R	0.02

REFERENCES

1. P. W. Gaiser, K. M. St. Germain, E. M. Twarog, G. A. Poe, W. Purdy, D. Richardson, W. Grossman, W. L. Jones, D. Spencer, G. Golba, J. Cleveland, L. Choy, R. M. Bevilacqua, and P. S. Chang, "The WindSat spaceborne polarimetric microwave radiometer: Sensor description and early orbit performance," *IEEE Trans. Geosci. Remote Sens.* **42**(11), 2347–2361 (Nov. 2004).

2. M. H. Bettenhausen and I. S. Adams, "The impact of passband characteristics on imaging microwave radiometer brightness temperatures over the ocean," *Radio Science* **48**(3), 352–357 (2013), ISSN 1944-799X, doi: 10.1002/rds.20041, URL `http://dx.doi.org/10.1002/rds.20041`.

3. J. A. Nelder and R. Mead, "A simplex method for function minimization," *The Computer Journal* **7**(4), 308–313 (1965), doi: 10.1093/comjnl/7.4.308, URL `http://comjnl.oxfordjournals.org/content/7/4/308.abstract`.

4. E. Jones, T. Oliphant, P. Peterson, et al., "SciPy: Open source scientific tools for Python" (2001–), URL `http://www.scipy.org/`.

5. V. Payne, E. Mlawer, K. Cady-Pereira, and J. Moncet, "Water vapor continuum absorption in the microwave," *IEEE Trans. Geosci. Remote Sens.* **49**(6), 2194 –2208 (2011), ISSN 0196-2892, doi: 10.1109/TGRS.2010.2091416.

6. A. P. Stogryn, "Equations for the permittivity of sea water," Report to the Naval Research Laboratory, Washington, D.C., Code 7223" (August 1997).

7. F. Chevallier, S. D. Michele, and A. P. McNally, "Diverse profile datasets from the ECMWF 91-level short-range forecasts," rept. NPWSAF-EC-TR-010, Sattelite Application Facility for Numerical Weather Prediction (2006).

8. M. H. Bettenhausen, C. K. Smith, R. M. Bevilacqua, N.-Y. Wang, P. W. Gaiser, and S. Cox, "A nonlinear optimization algorithm for WindSat wind vector retrievals," *IEEE Trans. Geosci. Remote Sens.* **44**(3), 597–610 (Mar. 2006).

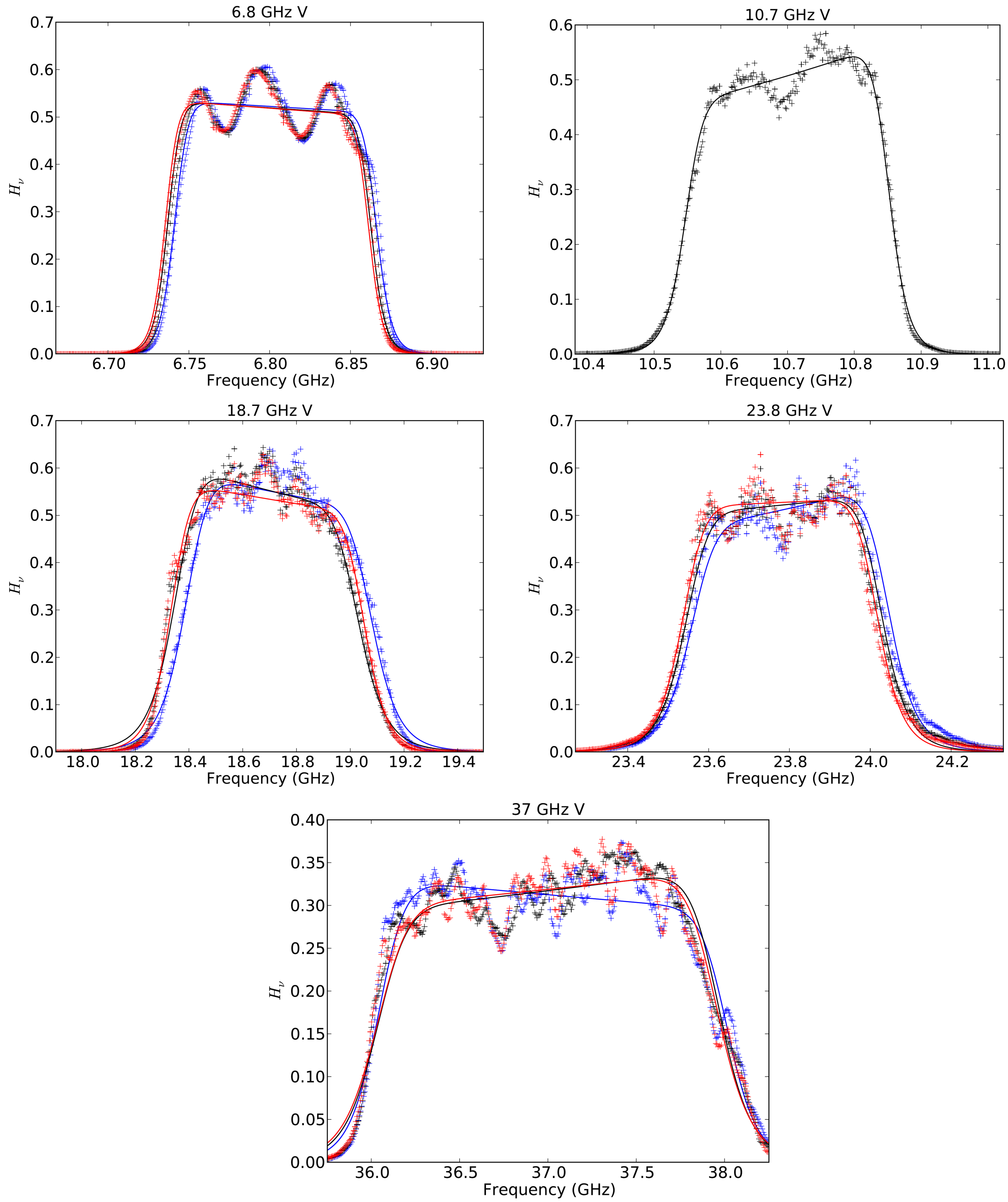

Fig. 1 — WindSat vertical polarization reciever passband responses. The measured responses are shown with the + signs and the solid lines are the functional fits in the form of Equation (1). The colors denote the receiver temperatures of 0 °C (blue), 25 °C (black) and 40 °C (red).

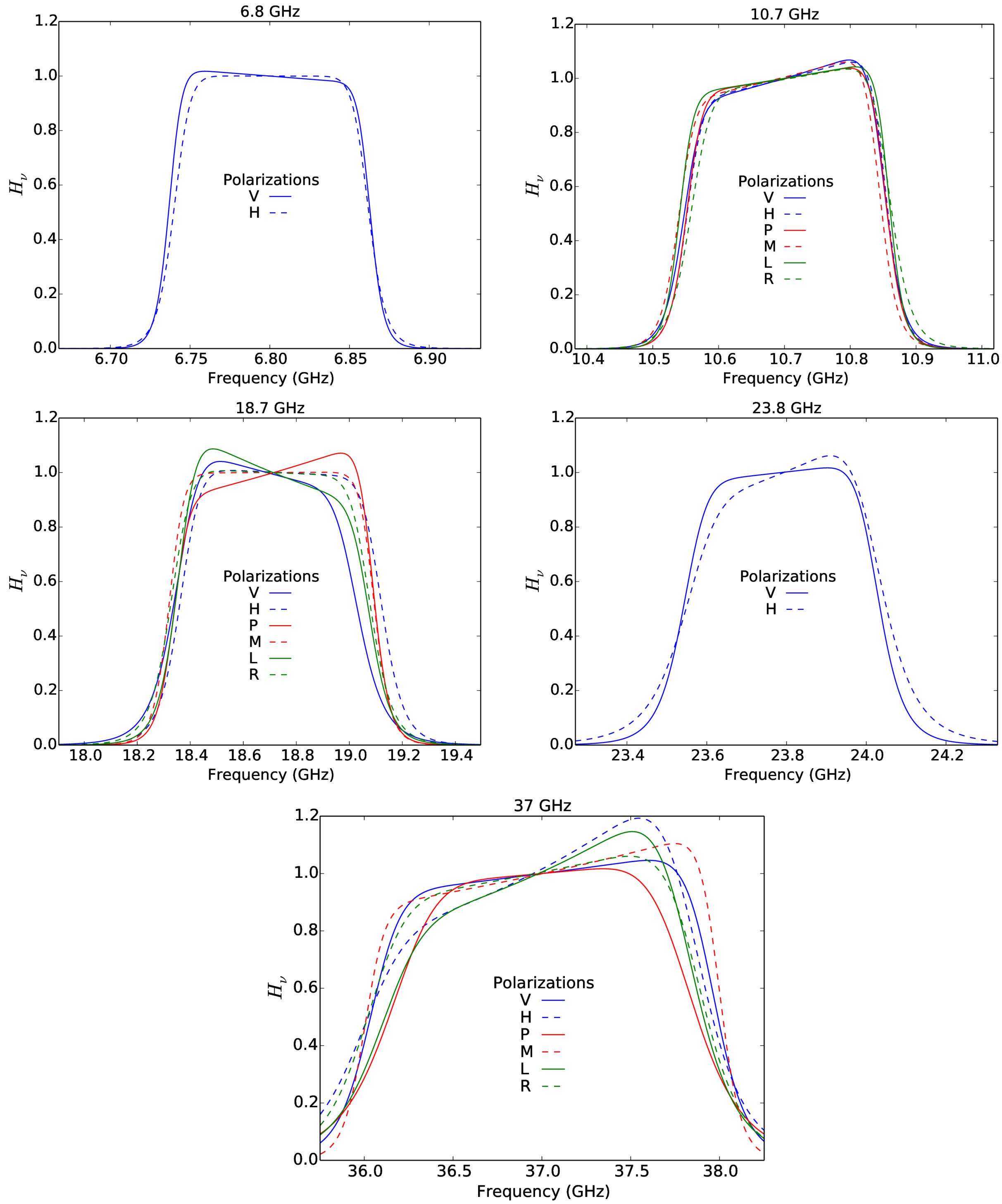

Fig. 2 — Optimized fits for the WindSat reciever passband responses measured at 25°C. All polarizations are shown for each WindSat frequency band.

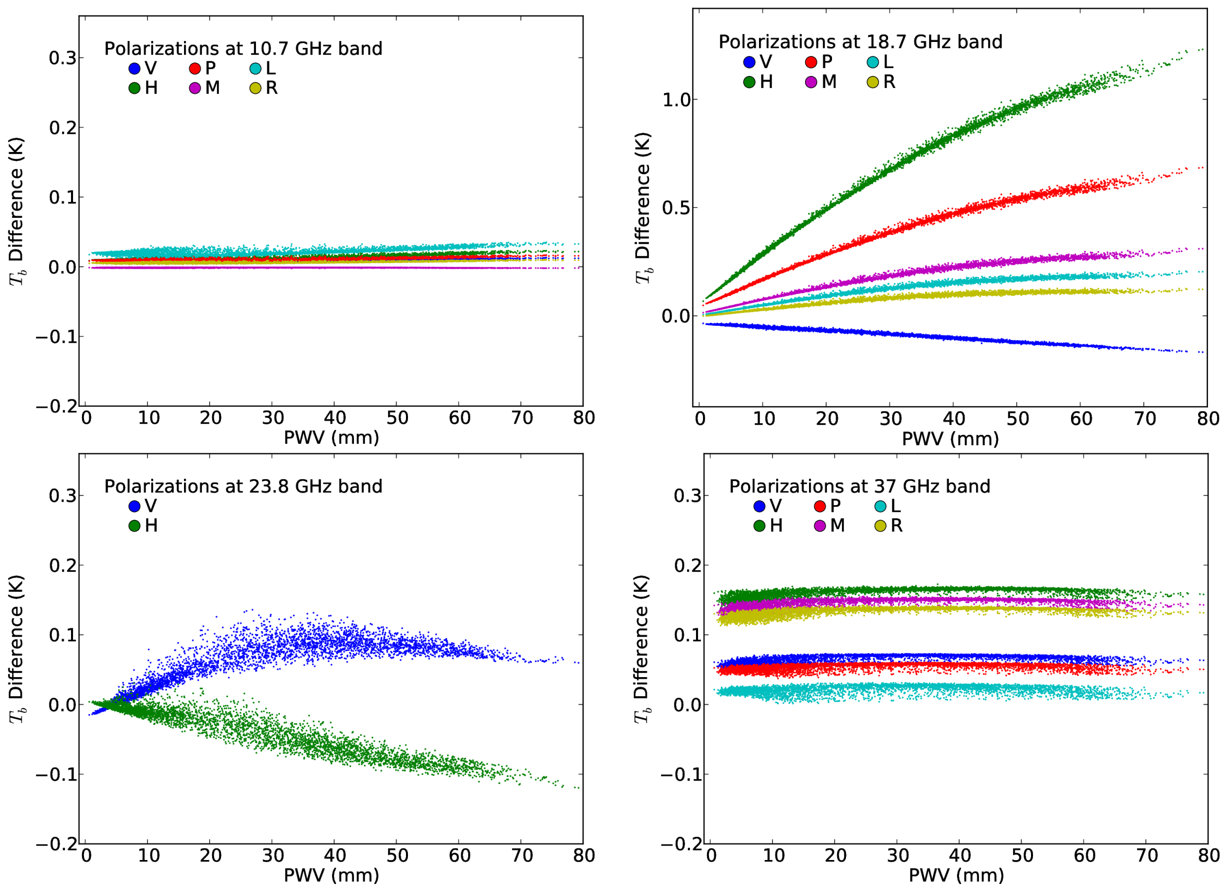

Fig. 3 — Modeled differences between the T_b's integrated over the measured passbands and the T_b's at the nominal center frequency for the respective bands ($T_b - T_{b,\,mono}$) versus precipitable water vapor (PWV).

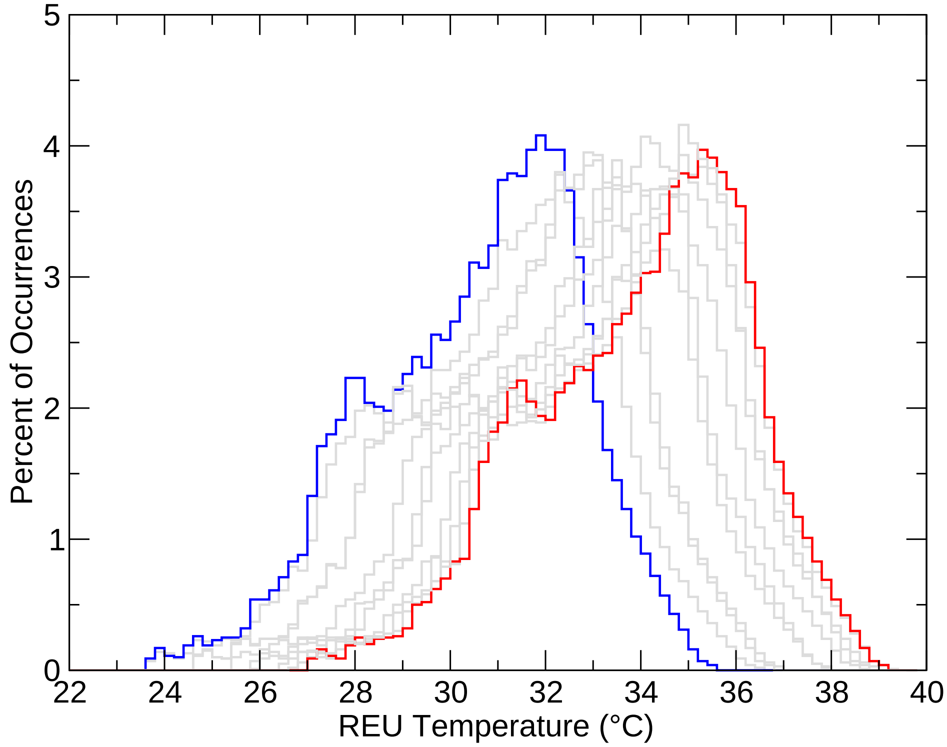

Fig. 4 — Distribution of REU temperature over the WindSat mission. Blue is for the 10.7 GHz V and H polarization REU and red is for the 37 GHz P and M polarization REU in 0.2 deg C bins. The remaining channels are shown in gray and exhibit similar shapes but and are bounded by the 10.7 GHz V and H polarization and 37 GHz P and M polarization under normal WindSat operating conditions.

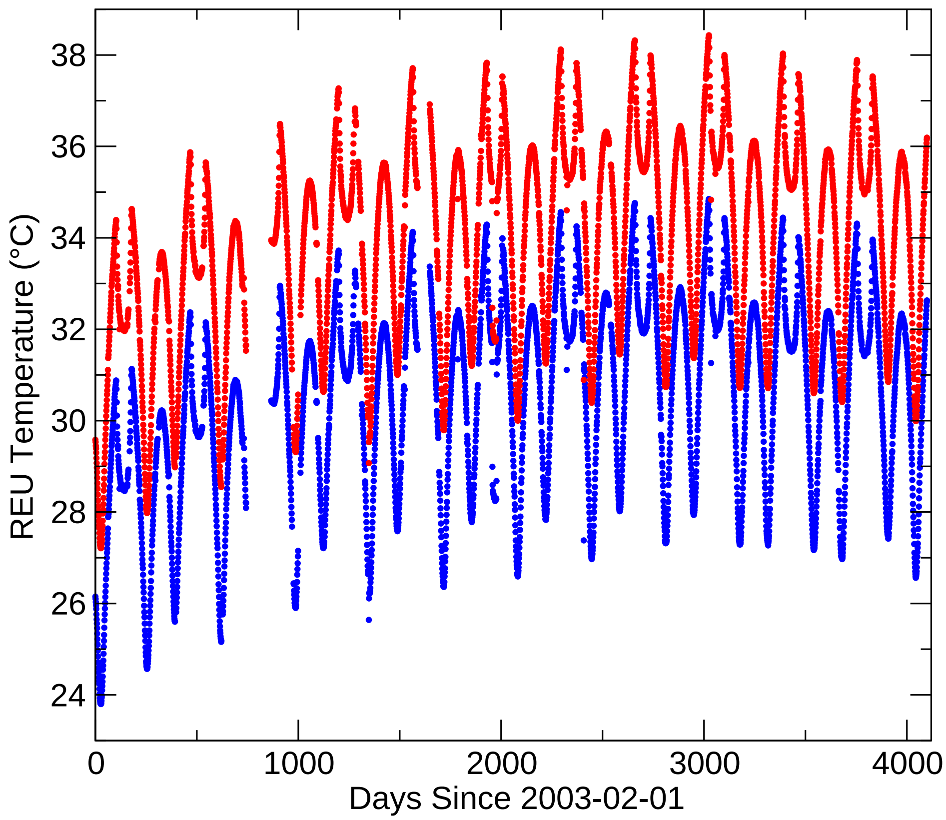

Fig. 5 — The daily mean REU temperature for 10.7 GHz V and H polarizations in blue and 37 GHz P and M polarizations in red from 2003-02-01 to 2014-04-23.

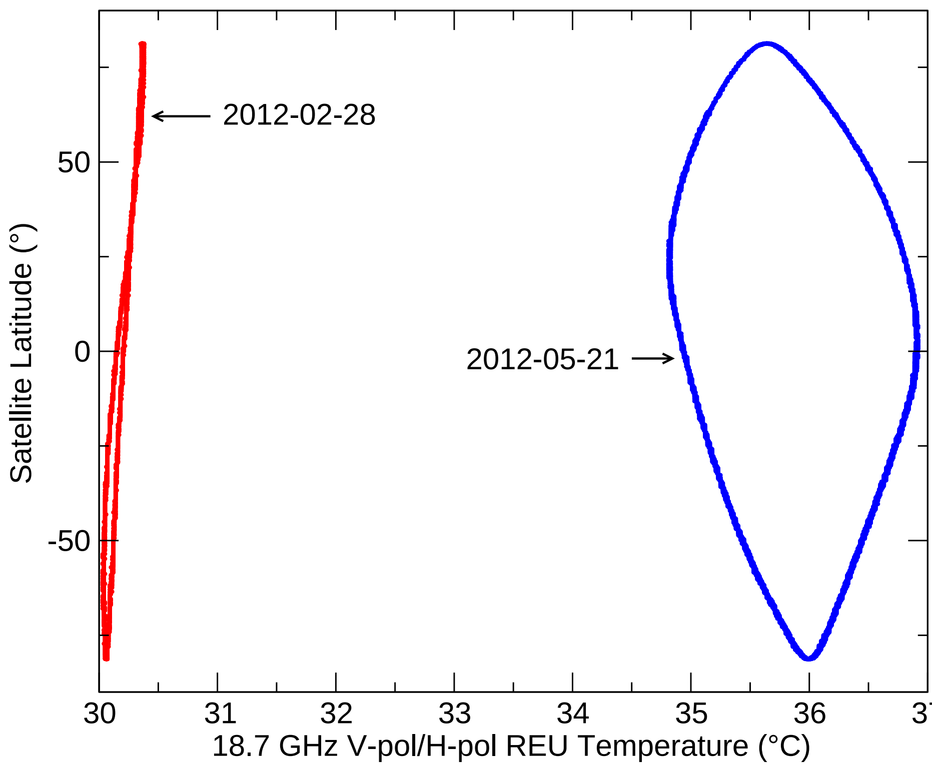

Fig. 6 — The REU temperature for the 18.7 GHz V and H polarizations for two orbits showing the change in temperature variation over the orbit. An orbit from 2012-02-28 is shown in red and an orbit from 2012-05-21 is shown in blue from 2012-05-21.